

INTEGRATION OF HYDRAULIC COMPONENTS IN A MULTIBODY FRAMEWORK FOR ROTORCRAFT ANALYSIS

Pierangelo Masarati[†], Gian Luca Ghiringhelli, Massimiliano Lanz,
and Paolo Mantegazza,
Dipartimento di Ingegneria Aerospaziale, Politecnico di Milano

Abstract

A framework for the integrated analysis of rotorcraft aeroservoelastic models, which considers the coupling of the rotorcraft aeroelasticity to the dynamics of hydraulic components related to rotorcraft controls, is presented. The hydraulic components are modeled in form of mixed lumped/distributed elements in a finite element way, which is integrated in a multibody framework for the modeling of the dynamics and of the aeroelasticity of rotorcrafts. An extensive validation of the formulation is presented; applications to realistic rotorcraft dynamics problems are outlined, including the active control of a tiltrotor wind-tunnel model based on the actuation of a conventional swashplate.

1 Introduction

The aerospace industry is moving towards the integrated analysis of multidisciplinary systems at every stage of the design and manufacturing process. The availability of commercial multibody analysis packages is pushing this approach; codes such as MDI's ADAMS, LMS' DADS, SAMCEF's MECANO and others offer the possibility of dealing with mechanical systems, and some of them provide some level of integration with hydraulic systems and with multidisciplinary systems in general. Most of them are oriented towards modeling the global behavior of those components, while some specialized hydraulics analysis codes can loosely interact with multibody codes. An example is Imagines, which provides some level of integration with ADAMS for the code AMESim in terms of user-defined linkable hydraulic component libraries.

In order to achieve the capability of investigating peculiar aspects of the dynamics of aerospace systems, a multibody analysis formulation and a multibody analysis code called MBDyn have been developed at the Department of Aerospace Engineering of the *Politecnico di Milano*. They have both been designed to be easily extended to the

integrated analysis of multidisciplinary systems.

The multibody formulation is based on the direct writing of the equilibrium equations of a set of discrete bodies, connected by algebraic constraints, in a *Lagrangian* multipliers approach, that leads to a system of Algebraic Differential Equations (DAE) of index 3. The multibody modeling technique allows an unparalleled freedom in assembling rather sophisticated mechanisms without any undue approximation in the kinematics of the constraints. A finite displacement and rotation, kinematically exact beam formulation, based on a finite volume model, allows to write the dynamics of the rotating blade in a straightforward manner.

This paper is focused on the integration of the components required to model hydraulic systems into the multibody analysis framework. The equations and the unknowns that model the hydraulic system are treated in analogy with the corresponding mechanical items. The time step integration is performed by an original implicit scheme based on a multistep formulation that allows unconditionally A/L -stable, second-order accurate integration, so the stiffness of the coupled system does not require any special care.

The main application is represented by the analysis of rotorcrafts. The control of the blade pitch is performed by modeling the kinematics of the complete control system, including the swashplate and the control links. The swashplate is actuated by means of a set of hydraulic actuators, whose dynamics is considered both from the mechanical and the hydraulic standpoint. The actuators are fed by means of a detailed hydraulic circuit, including servovalves, pipelines, accumulators, pressure and flow generators. The dynamics of the hydraulic

[†]Corresponding Author
via La Masa, 34 — 20156 Milano, Italy
Tel.: +39(02)2399 8365
Fax: +39(02)2399 8334
E-mail: masarati@aero.polimi.it

Presented at the 26th European Rotorcraft Forum,
26–29 September 2000, The Hague, The Netherlands

components is accounted for, including the effects of fluid compressibility and of *Reynolds* number in the computation of the viscous losses inside the circuit. Both the transfer function approach and the detailed, nonlinear modeling of the physics of the servovalves have been exploited. While the two approaches may only slightly differ when the system dynamics are addressed, the latter allows a better insight into the hydraulic system when its design is specifically addressed. Moreover, the thorough modeling of the physical components allows the designer to assess the performances and the limitations of the system in a wide range of operating conditions outside the design point.

2 Multibody Formulation

A multibody system, in a conventional sense, is intended as a collection of bodies that hold the degrees of freedom of the system. They can be connected by means of kinematic or flexible constraints. Because the bodies in principle are considered independent, they are allowed to undergo large, finite *absolute* displacements and rotations, the latter requiring accurate description owing to the intrinsic nonlinearity of finite rotation parametrizations. Moreover, the configuration history of the system may also result in large *relative* displacements and rotations, which means large, finite strains in flexible structural components.

In a broader sense, a multibody system may be viewed as a *global modeling system*, which consists in modeling an integrated (aero)-(thermo)-servoelastic nonlinear system without any undue approximation in the description of its kinematics. In this sense, the multibody approach may be intended as nonlinear Finite Elements applied to servomechanical problems, where the description of the exact kinematics is emphasized.

A multistep, implicit second-order accurate integration scheme has been used to integrate the initial value DAE system that results from the multibody modeling of the problem. It allows to control the amount of algorithmic dissipation introduced into the computation. The formula is

$$\begin{aligned}\dot{y}_n &= -\frac{12}{h}y_{n-1} + \frac{12}{h}y_{n-2} + 8\dot{y}_{n-1} + 5\dot{y}_{n-2}, \\ y_n &= (1-\alpha)y_{n-1} + \alpha y_{n-2} + \frac{h}{2}(1+2\delta)\dot{y}_n \\ &\quad + \frac{h}{2}(1+\alpha-4\delta)\dot{y}_{n-1} + \frac{h}{2}(\alpha+2\delta)\dot{y}_{n-2},\end{aligned}$$

where h is the time step. The derivative of the state is predicted with a cubic extrapolation, while

the state itself is predicted by a second-order accurate formula, whose coefficients can be expressed as functions of the desired asymptotic spectral radius for the numerical solution:

$$\begin{aligned}\alpha &= \frac{4\rho_\infty^2 - (1-\rho_\infty)^2}{4 - (1-\rho_\infty)^2}, \\ \delta &= \frac{1}{2} \frac{(1-\rho_\infty)^2}{4 - (1-\rho_\infty)^2}.\end{aligned}$$

The formula has been derived from a broader class of multistep numerical integration schemes; it represents a good compromise between accuracy and implementability in a general multidisciplinary multibody formulation [1].

2.1 Rigid Body Dynamics

The equilibrium equations are directly used to describe the dynamics of a rigid body. Consider a body of mass m , with first- and second-order inertia moments S and J , whose configuration is described by the position x and the orientation R , and whose angular velocity is $\omega \times = \dot{R}R^T$; the momentum and the momenta moment, with respect to the body reference point, are:

$$\begin{aligned}\beta &= m\dot{x} - S \times \omega, \\ \gamma &= S \times \dot{x} + J\omega.\end{aligned}$$

Their time derivative yields the inertia force and couple contribution to the equilibrium equations of the body:

$$\begin{aligned}\dot{\beta} &= F, \\ \dot{\gamma} + \dot{x} \times \beta &= M.\end{aligned}$$

A detailed description of the formulation can be found in [2, 3, 4].

2.2 Kinematic Constraints

The kinematic constraints are introduced by means of algebraic equations in a *Lagrangian Multipliers* way, depending on the kinematics of the bodies. The multipliers represent the reacting forces, which directly contribute to the equilibrium of the constrained bodies. Consider for instance a spherical hinge joint, which basically forces two nodes to share a point. To make the joint general, consider a pair of constraint points, x_{c1} , x_{c2} , that are offset from the body reference points: $x_{ci} = x_i + f_i$, where f_i is an offset vector that for simplicity is assumed to be constant, i.e. rigid and independent of time, in the body reference frame. The constraint equation is

$$x_2 + f_2 - x_1 - f_1 = 0.$$

It implies the existence of three reaction unknowns, the reaction forces F , that are applied to the bodies at the constraint points; as a consequence, the resulting forces and couples on the bodies are:

$$\begin{aligned} F_1 &= F, \\ F_2 &= -F, \\ M_1 &= f_1 \times F, \\ M_2 &= -f_2 \times F. \end{aligned}$$

A complementary constraint is the one that enforces the orthogonality of two arbitrary unit vectors, e_1 , e_2 , that are fixed in the reference frames of two bodies. The (scalar) constraint equation is

$$e_1^T e_2 = 0$$

It results in a scalar couple, c , that acts in the direction normal to the plane generated by the two orthogonal vectors, namely

$$\begin{aligned} M_1 &= (e_1 \times e_2) c, \\ M_2 &= -M_1. \end{aligned}$$

2.3 Flexible Constraints

Under the definition of flexible constraints both lumped elastic and viscoelastic elements and Finite Element-like discrete deformable elements are collected. The present formulation entails a finite volume beam model and a general flexible body based on the superimposition of a rigid body motion and of a linear combination of flexible modes, computed by means of a linear finite element modal analysis, and possibly of static shapes. The flexibility is handled in terms of “flexible constraints”, since the multibody philosophy interprets flexibility as a source of internal forces that tie otherwise independent bodies together. From an operational standpoint, however, the trends of flexibility implementation in multibody analysis move towards true nonlinear finite elements; the same approach has been followed in this work. A detailed description of the finite volume beam formulation, which is key to the capabilities of the multibody analysis presented in this work, can be found in [3].

3 Hydraulic Formulation

The hydraulic system is modeled in form of a hydraulic network, which is discretized in a finite element manner. The nodal pressures are considered as primary algebraic unknowns, and the conjugated equations involve the nodal flux balance. Wherever the time derivative of the pressure is required to

describe the dynamics of a component, it is considered as an internal differential state p_i of the related element, and an algebraic equation is written to relate it to the pressures p_n at the boundaries of the element, namely

$$p_i = f(p_n).$$

Most of the hydraulic components have been modeled as lumped elements: the minor losses, the orifice, the accumulator, the reservoir, and the valves. Particular care has been taken in modeling the pipelines; a dedicated finite volume implementation is here presented for the characterization of a pipe that accounts for compressibility as well as viscosity. Thanks to the particular nature of the multibody framework the hydraulic system has been implemented in, advantage has been taken of the *Object Oriented* pre-existing environment by resorting to a layered scheme. Utility objects that implement many simple elements (linear losses, pressure and flux generators) were inherited from an existing multi-purpose element library.

3.1 Generic Hydraulic Fluid

The hydraulic fluid properties object is shared by all the hydraulic elements, and allows the user to introduce customized fluid constitutive laws and properties without interfering with the implementation of the elements. The most general constitutive law is implemented in principle, because only its local linearization is required during the solution:

$$\rho = \rho(p, \dots), \quad \frac{\partial \rho}{\partial p} = \frac{\partial \rho(p, \dots)}{\partial p}.$$

The linearized compressible fluid, which is characterized by the widely used linear approximation of the relationship between the fluid density, ρ , and the local pressure p , is a typical example:

$$\rho = \rho_0 + \frac{\partial \rho}{\partial p} (p - p_0), \quad (1)$$

where the bulk modulus β is used in

$$\frac{\partial \rho}{\partial p} = \frac{\rho_0}{\beta}.$$

Each element uses a general *Application Programming Interface* (API) to ask the *Fluid Object* for the value of the density and for its pressure rate as functions of the local pressure; in C++ notation, a pure virtual base class for a pressure dependent hydraulic fluid is shown in Figure 1. The *methods* that do not require the pressure in input simply yield the reference values of density and density rate;

```

class HydraulicFluid {
    // ...
public:
    virtual Real GetDensity(void) const = 0;
    virtual Real GetDensity(const Real & Pressure) const = 0;
    virtual Real GetDensityDPressure(void) const = 0;
    virtual Real GetDensityDPressure(const Real & Pressure) const = 0;
    // ...
};

```

Figure 1: Hydraulic Fluid Pure Virtual Class Declaration

they are used by those elements that do not handle the compressibility. Those in turn that require the pressure do yield the actual density and density rate regardless of the underlying fluid model. The effectiveness of this approach has been highlighted by the recent addition of a simplified cavitation model to the standard linear fluid, which required no modification of the hydraulic element library at all:

$$\rho = \frac{\rho_0}{2} (1 + \tanh(\alpha(p - p_0))) + \frac{\rho_0}{\beta} \text{ramp}(p - p_0).$$

The use of such a simplified constitutive law does not prevent the solution from encountering negative pressures in critical cases, but it partially cures the problem, and in general it may warn the user of a possible misuse of the analysis scheme.

3.2 Boundary Conditions

Typical hydraulic network boundary conditions involve 1) the enforcement of the pressure at some nodes, and 2) the imposition of the inflow at other nodes.

Since the nodal pressures are the main hydraulic unknowns, the pressure at a node can be enforced by using an algebraic constraint in the form:

$$p_n = p_0,$$

where the nodal pressure p_n is required to match the desired value p_0 (which may depend on time or on other states), in analogy with the enforcement of a displacement in a structural model. At the same time, an unknown reaction flux q_0 , originating from the ideal “pressure generator”, must be added to the node balance equation.

The input of an exogenous flux q_0 at a node is imposed by simply adding it to the node balance equation, in analogy with the imposition of an external force in a displacement-based structural model.

3.3 General Lumped Elements

Concentrated losses, orifices, the accumulator and the reservoir have been modeled as lumped elements. Their implementation is relatively straightforward, so it has not been reported here for simplicity. Interested readers may refer to any basic text on hydraulic systems [5].

3.4 Pipelines

Consider the mass conservation and the momentum balance equations for a one-dimensional flow:

$$\frac{D}{Dt}(dm) = 0, \quad (2)$$

$$\frac{D}{Dt}(dQ) = df. \quad (3)$$

When a rigid pipe is considered, the total derivative D/Dt of the test mass $dm = \rho A dx$ of Equation (2) yields

$$\frac{D}{Dt}(dm) = \frac{\partial}{\partial t}(dm) + v \frac{\partial}{\partial x}(dm),$$

which results in

$$q_{/x} + A\rho_{/t} = 0,$$

where $q = \rho A v$ is the mass flux. Consider now the momentum equation (3); the total derivative of the momentum $dQ = v dm$ yields

$$\frac{D}{Dt}(dQ) = (q_{/t} + (qv)_{/x}) dx,$$

while the pressure gradient and the viscous contributions can be isolated from the force per unit length on the right hand side:

$$df = -Adp + f_v dx + df^*,$$

so, by neglecting the deformability of the pipe and the extra forces df^* acting on the fluid, the momentum balance equation yields

$$q_{/t} + (qv + Ap)_{/x} = f_v,$$

which can be reduced to the pressure and flux unknowns simply by recalling the definition of the flux:

$$q_{/t} + \left(\frac{q^2}{\rho A} + Ap \right)_{/x} = f_v.$$

A flexible pipe has been considered as well; the formulation is not reported for simplicity, because such a level of detail is required only for very specialized problems, and a first approximation can be obtained by altering the bulk modulus of the fluid. The pipe is discretized by considering a finite volume approach, based on the use of constant stepwise (*Heavyside*) test functions with arbitrary trial functions. In the present case, linear trial functions have been considered both for the flux and for the pressure:

$$\begin{aligned} q(x) &= \left[\frac{1-\xi}{2} \quad \frac{1+\xi}{2} \right] \begin{Bmatrix} q_1 \\ q_2 \end{Bmatrix}, \\ p(x) &= \left[\frac{1-\xi}{2} \quad \frac{1+\xi}{2} \right] \begin{Bmatrix} p_1 \\ p_2 \end{Bmatrix}, \end{aligned}$$

with $\xi = \xi(x) \in [-1, 1]$ and $d\xi/dx = 2/(b-a)$. The discrete form of the pipe equations results in

$$\begin{aligned} q(b) - q(a) &= - \int_a^b \frac{\partial \rho}{\partial p} p_{/t} dx, \\ \frac{b-a}{2} (q(b)_{/t} + q(a)_{/t}) + \left(\frac{q(b)^2}{\rho(b)A} + Ap(b) \right) \\ &- \left(\frac{q(a)^2}{\rho(a)A} + Ap(a) \right) = \int_a^b f_v dx; \end{aligned}$$

by dividing the pipe in two portions, and by considering the domains $[-1, 0]$ and $[0, 1]$ for ξ in each portion, the discrete equations of the finite volume pipe become

$$\begin{aligned} -\frac{1}{2} (q_1 + q_2) - \frac{\partial \rho(-1/2) L}{\partial p} \frac{1}{8} (3\dot{p}_1 + \dot{p}_2) &= \phi_1, \\ \frac{1}{2} (q_1 + q_2) - \frac{\partial \rho(1/2) L}{\partial p} \frac{1}{8} (\dot{p}_1 + 3\dot{p}_2) &= \phi_2, \\ \frac{L}{8} (3\dot{q}_1 + \dot{q}_2) + \frac{(q_1 + q_2)^2}{4\rho(0)A} - \frac{q_1^2}{\rho(-1)A} \\ &+ \frac{A}{2} (p_2 - p_1) = \frac{L}{2} \int_{-1}^0 f_v d\xi, \\ \frac{L}{8} (\dot{q}_1 + 3\dot{q}_2) + \frac{q_2^2}{\rho(1)A} - \frac{(q_1 + q_2)^2}{4\rho(0)A} \\ &+ \frac{A}{2} (p_2 - p_1) = \frac{L}{2} \int_0^1 f_v d\xi, \end{aligned}$$

where ϕ_1 and ϕ_2 are the contributions of the two portions of pipe to the respective nodal flux balance equations. The integral of the time derivative of the

density is numerically computed, although, when the usual linearized form of Equation 1 is considered, a closed form solution may be easily obtained. The integral of the viscous forces per unit length is numerically performed as well, accounting for the flow regime in the pipe as function of the *Reynolds* number. In fact, for the forces per unit length, the dependency on the flux is considered linear for $0 < Re < 2000$, and quadratic for $Re > 4000$, while a polynomial fitting of the transition behavior, accounting also for the rate of the *Reynolds* number, is modeled for $2000 < Re < 4000$.

3.5 Actuators

The actuator has been modeled in the spirit of the multibody approach by combining a set of elementary parts. The mechanical part of the device is obtained by assembling conventional structural parts, namely two rigid bodies connected by a joint that allows relative sliding and axial rotation. Mechanical friction between the parts, even dependent on the reaction forces, can be easily added, although at present none has been considered.

The relative kinematics, namely the elongation and its time rate, are used to compute the volume of the chambers and the volumetric flux. The two bodies share an axis as a consequence of the application of the slide constraint; the distance between the bodies is thus

$$d = e_1^T (x_2 + f_2 - x_1 - f_1),$$

where e_1 is the unit vector oriented as the axis of the actuator; it is arbitrarily related to the first body, with no loss in generality, owing to the sliding constraint. A general configuration, with the actuator axis offset from the nodes by the relative positions f_1 and f_2 is considered to allow as much freedom as possible in modeling the system. The time derivative of the distance yields the relative velocity:

$$\begin{aligned} \dot{d} &= e^T (\dot{x}_2 + \omega_2 \times f_2 \\ &- \dot{x}_1 - \omega_1 \times (x_2 + f_2 - x_1)). \end{aligned}$$

As a result, the volumes in the two chambers are

$$\begin{aligned} V_1 &= A_1 (L_1 + d), \\ V_2 &= A_2 (L_2 - d), \end{aligned}$$

and the fluxes are

$$\begin{aligned} q_1 &= \rho_1 A_1 \dot{d} + V_1 \frac{\partial \rho}{\partial p} \dot{p}_1, \\ q_2 &= -\rho_2 A_2 \dot{d} + V_2 \frac{\partial \rho}{\partial p} \dot{p}_2. \end{aligned}$$

No built-in leakage between the two chambers has been modeled; in fact, a leakage can easily be added by connecting the two pressure nodes that describe the lumped chambers with a general purpose minor loss element.

The pressures in the chambers are used to compute the forces and the couples that the actuator applies to the two related bodies. They result in:

$$\begin{aligned} F_1 &= e_1 (A_1 p_1 - A_2 p_2), \\ F_2 &= -F_1, \\ M_1 &= f_1 \times F_1, \\ M_2 &= f_2 \times F_2. \end{aligned}$$

Extra structural forces, such as inertia and friction, can be separately added by combining appropriate structural elements.

3.6 Control Valves

The actuator can be connected to a hydraulic network at the pressure nodes related to the two chambers. A significant case is that of a network composed of an actuator connected to a servovalve by means of pipelines. A servovalve consists in a set of equations that distribute the input and output flows to a subcircuit based on the value of a parameter related to the position of the mobile part of the valve. Its dynamics can be modeled as well, leading to a dynamic valve model. In usual implementations the dynamics of the valve is accounted for by means of transfer functions, which imply a linearized model; this is very useful when the initial design of the hydraulic system is considered, but it may represent an oversimplifying assumption at a more advanced design stage. In the present case, the dynamics of the valve is directly written, accounting for all the nonlinear terms related to the dynamics of the fluid.

The valve uses four pressure nodes, that can be arbitrarily connected, depending on the value of its state. The subscripts refer to the symbols used in Figure 2. The cross-sections of the orifices are

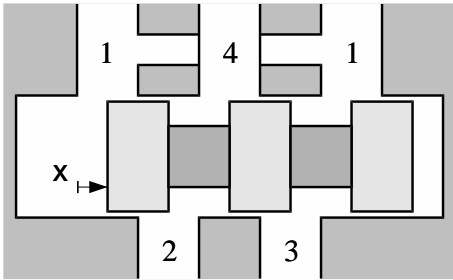


Figure 2: Control Valve

$$\begin{aligned} A_1 &= A_{1m} + w \text{ ramp}(x) \\ A_2 &= A_{2m} + w \text{ ramp}(-x) \\ A_3 &= A_{3m} + w \text{ ramp}(x) \\ A_4 &= A_{4m} + w \text{ ramp}(-x) \end{aligned}$$

where A_{im} indicates a residual section that accounts for leakages, x is the position of the mobile part of the valve and w is the transverse dimension of the orifices. By assuming a turbulent flow across the orifices of the valve, the fluxes at the four nodes are defined as

$$\begin{aligned} q_1 &= -C_d A_2 \sqrt{2\rho |p_1 - p_3|} \text{sign}(p_1 - p_3) \\ &\quad - C_d A_1 \sqrt{2\rho |p_1 - p_2|} \text{sign}(p_1 - p_2), \\ q_2 &= C_d A_1 \sqrt{2\rho |p_1 - p_2|} \text{sign}(p_1 - p_2) \\ &\quad - C_d A_4 \sqrt{2\rho |p_2 - p_4|} \text{sign}(p_2 - p_4), \\ q_3 &= C_d A_2 \sqrt{2\rho |p_1 - p_3|} \text{sign}(p_1 - p_3) \\ &\quad - C_d A_3 \sqrt{2\rho |p_3 - p_4|} \text{sign}(p_3 - p_4), \\ q_4 &= -C_d A_3 \sqrt{2\rho |p_3 - p_4|} \text{sign}(p_3 - p_4) \\ &\quad - C_d A_4 \sqrt{2\rho |p_2 - p_4|} \text{sign}(p_2 - p_4). \end{aligned}$$

The dynamics of the valve is described [5] by

$$\begin{aligned} m\ddot{x} + \left(0.4DwC_d\sqrt{\rho\Delta p}\right)\dot{x} \\ + (0.43w\Delta p + k)x = F; \end{aligned} \quad (4)$$

it accounts for the suction effect at the openings in the chambers as well as for the viscosity due to the motion of the valve body. A structural spring k has been added for completeness.

4 Results

4.1 Validation of the Formulation

The hydraulic components have been independently validated by performing thorough unit tests; only the case of the pipe that accounts for fluid compressibility and viscosity is presented for simplicity. Consider a pipe of length $l = 19.74$ m, diameter $d = 12.32\text{e-}3$ m, filled with a fluid of density $\rho = 870$ kg/m³, bulk modulus $\beta = 1705$ MPa and viscosity $\mu = 0.0696$ kg·s/m, which is loaded by a stepwise flux $q = 1.\text{e-}3$ for $1.\text{e-}4$ seconds at one end. The pressure at the other end is free, which means that the pipe is perfectly sealed. The problem has been discussed in the literature; a solution based on a spectral formulation of the problem has been proposed in [6], compared to other integration methods. The solution is represented by a train of waves that travel back and forth from the loaded end, as clearly shown in Figure 3, where the pressure as function of time and position is depicted

Table 1: Hydraulic Circuit Properties

Kinematic Viscosity	80	$\mu\text{m}^2/\text{s}$
Density	870	kg/m^3
Sound Speed	1400	m/s
Pipe Radius	0.006	m
Orifice Diameter	0.006	m
Orifice Coefficient	0.6	
Actuator Area	0.01	m^2
Actuator Volume	0.001	m^3

for the first 0.2 s of simulation. The present solution showed to be slightly dependent on the spatial resolution (in this case 20 pipe elements have been used, but the 10 element solution does not appreciably differ), while a higher dependence on the time step and on the algorithmic dissipation of the integration scheme has been noticed. The use of an implicit integration scheme with algorithmic dissipation allows to damp the oscillatory response known as *Gibbs* phenomenon, that is related to the high stiffness of the discretized problem.

4.2 Integrated Analysis

A simple servomechanical system, which has been presented in [7], is considered first. It is composed of a straight, uniform beam, pinned at one end and actuated by a hydraulic actuator attached to a simple hydraulic circuit; a sketch is shown in Figure 4. The beam is 2 m long, with linear density and inertia moments $m = 13 \text{ kg}/\text{m}$ and $\rho I_A = 1.7\text{e-}3 \text{ kg}\cdot\text{m}$. An axial stiffness $EA = 3.36\text{e}8 \text{ N}$ has been considered, together with shear and bending stiffnesses $GA = 1.47\text{e}8 \text{ N}$ and $EJ = 8.96\text{e}3 \text{ N}\cdot\text{m}^2$. The circuit is represented by a 20 m long pipeline that brings the hydraulic fluid to one chamber of the actuator; an orifice is placed just before the actuator. The properties of the circuit are reported in Table 1. No external forces are considered; the system is loaded by assigning the flow at the beginning of

Pressure, MPa

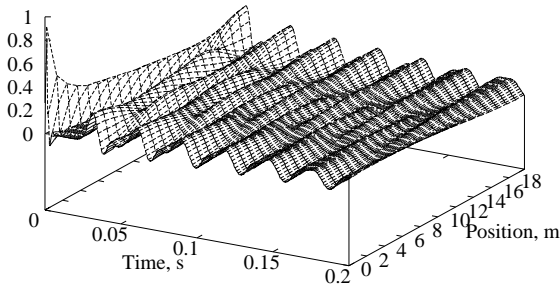


Figure 3: Pressure Waves in a Pipe

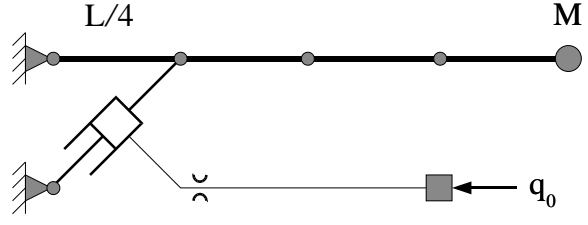


Figure 4: Integrated Analysis: Model

the pipeline, which is linearly increased from zero to $2\text{e-}3 \text{ m}^3/\text{s}$ in one second, and then goes back to zero in the following second. As a result, the tip of the beam is raised. All the hydraulic components account for fluid compressibility and for the *Reynolds* number in computing the viscous losses, and the transition from laminar to turbulent flow is considered as well, as opposed to Reference [7] where the fluid was supposed to assume laminar and turbulent behavior in the pipeline and in the orifice, respectively. The beam has been modeled with finite volume beam elements; the resulting bending moment at midspan is reported in Figure 5, while Figure 6 presents the movement of the beam with a 0.2 s sampling rate. Figure 7 shows the pressure

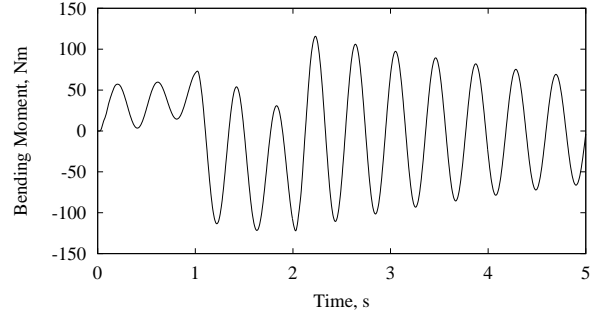


Figure 5: Integrated Analysis: Midspan Bending

distribution in the pipe. Some differences in the dynamics of the system with the results reported in [7] can be appreciated, but the overall agreement is fairly good. The solution is nearly insensitive to the time step and to the algorithmic dissipation level; a spectral radius of $\rho = 0.6$, which proved to be a good compromise between stability and accuracy of the computation, has been used. The analysis has been performed with a $5\text{e-}3 \text{ s}$ time step, which is slightly longer than the average (supposedly variable) one used in [7].

4.3 Tiltrotor Control

A multibody model of the WRATS tiltrotor wind-tunnel model is considered next [2, 8]. It is cur-

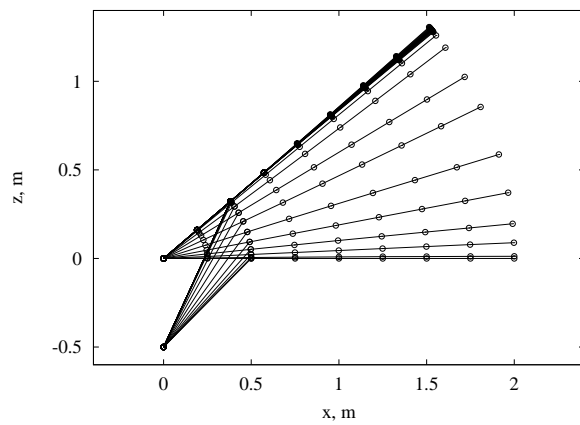


Figure 6: Integrated Analysis: Beam Movement

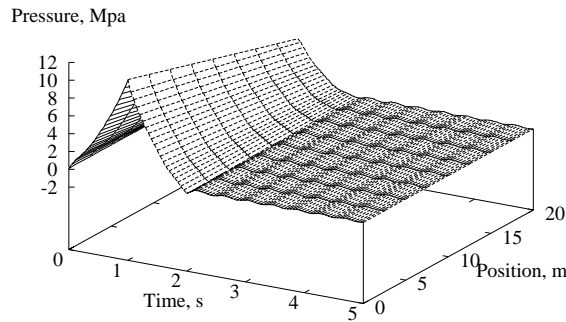


Figure 7: Integrated Analysis: Pressure Distribution in the Pipe

rently used at the NASA Langley Research Center to investigate the tiltrotor technology after serving in the past for the development of the V-22 Osprey [9]. The analytical model uses beam elements to model both the flexible wing and the rotor blades. The conversion mechanism, the hub with the gimbal joint, the swashplate mechanism and the kinematics of the blade pitch are modelled by means of algebraic constraints. The strip theory is considered for the aerodynamics of the wing and of the blades, with a dynamic inflow model. The swashplate is actuated by means of three high-frequency hydraulic actuators, whose behavior has been previously simulated by variable length joints; the desired lengths were filtered by means of a transfer function [8]. The numerical model has been upgraded by adding hydraulic actuators controlled by servovalves; thanks to the integrated modeling of the hydraulics, more realistic dynamics of the actuators have been achieved. A multilayered control scheme has been implemented. The hydraulic components of the flight control system, namely the actuators, the control valves and the pipelines, are separately modeled. A set of PID controllers takes care of enforcing the desired position of the actua-

tors, based on the errors between their desired and measured elongations. A picture of the model, elaborated with ADAMS/View, is shown in Figure 8, while Figure 9 contains a detail of the controls.

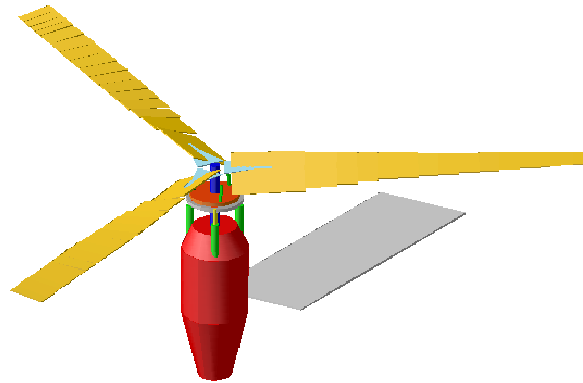


Figure 8: Tiltrotor Model

Some maneuver simulations have been performed,

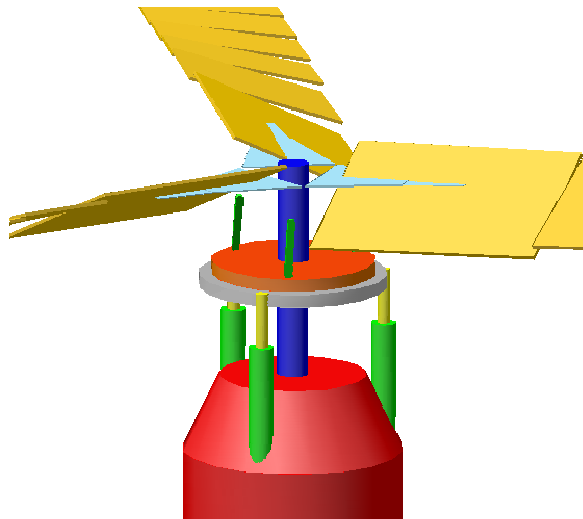


Figure 9: Tiltrotor Controls Detail

to exemplify the flexibility and the completeness of the analyses that can be performed. It is worth stressing that, due to the sophistication of the modelling, the direct computation of a trimmed flight condition is hardly achievable. As a result, steady state conditions are reached by simulating a complete test session, consisting in the wind-up of the rotor, during which both the collective controls, and the tunnel airspeed in case of forward flight analyses, are raised to their nominal value. The actual simulation follows, during which controls or external excitations are applied, and the response of the system is evaluated. A collective sweep, and a cyclic fore/aft pitch control are applied to the model in hover flight conditions. The results in terms of ro-

tor thrust and of wing internal couples are reported in Figures 10 and 11. Figure 12 shows the pres-

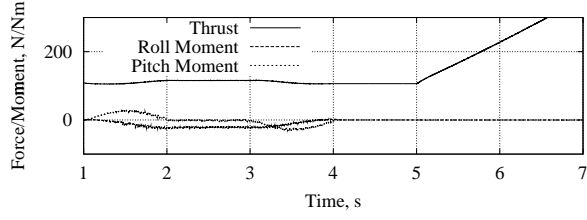


Figure 10: Thrust and Aerodynamic Moments

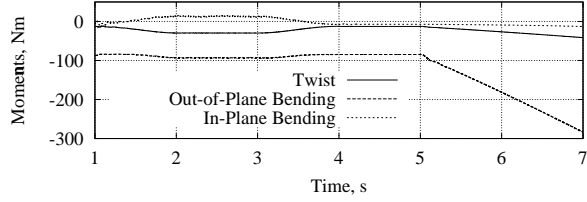


Figure 11: Wing Root Internal Couples

sure in the two chambers of an actuator during the maneuvers. The oscillations during the transients are related to the dynamics of the control of the valves, which are required to supply very small displacements and thus are working in a range of high nonlinearity, as can be noticed from Equation 4.

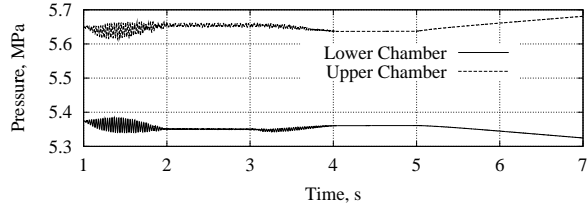


Figure 12: Pressure in an Actuator

A high-level *Generalized Predictive Control* scheme [10] accounts for superimposing a control signal on the open-loop controls set by the pilot, to alter the flight performances of the system. The GPC controller has been implemented in an adaptive scheme that aims at stabilizing the system with respect to the rotor-pylon flutter mode. Both gust load reduction and system stabilization have been addressed, and interesting results have been recently achieved with the transfer function models [8]; they are substantially confirmed by the present work in case of detailed modelling of the hydraulics. The stability augmentation of the system in forward flight has been addressed in the subsequent set of analyses. A flutter speed of 173 Kts with 52.5 deg collective has been found for the model without the hydraulic

system. Such limit speed has been substantially confirmed when the hydraulics are modelled.

The stability augmentation system is based on the measure of the strains at the root of the wing that correspond to in- and out-of-plane bending and torsion, plus the fore/aft, normal and twist accelerations at the pylon. The controls are directly added to the desired elongations of the three swashplate actuators, which are fed to the valve controllers.

The model has been trimmed in forward flight to a speed of 172 Kts with 52 deg of collective pitch; the system has been identified for a total time of 10 s, and during the last 5 s the controller has been activated. Then the tunnel speed has been raised at a 1 Kts/s ratio up to 212 Kts (123% of the flutter speed), together with the baseline collective to maintain about zero thrust, without any loss of stability of the system. Figure 13 shows the resulting wing out-of-plane bending, while Figure 14 contains the desired and measured elongations of one actuator during the simulation. Notice that the actuator

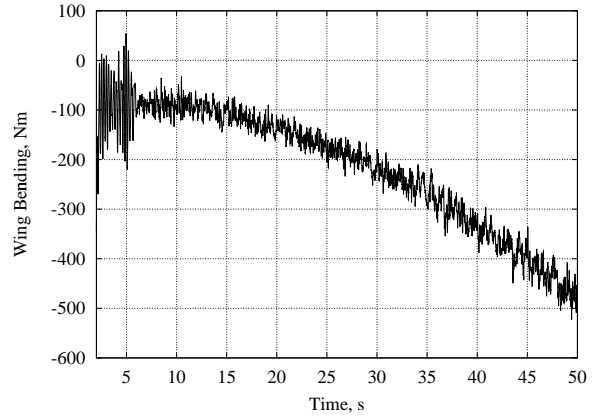


Figure 13: Tiltrotor Flutter Suppression, Wing Out-of-Plane Bending

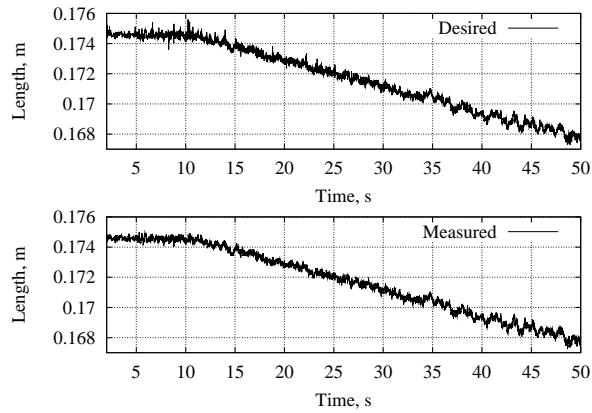


Figure 14: Tiltrotor Flutter Suppression, Actuator Elongation

is shortening to yield a higher collective because the pitch horn has been placed behind the blade, in order to obtain a negative pitch-flap coupling ($\delta_3 \cong -15$ deg). The comparatively high noise level is related to the persistent excitation that the adaptive controller requires to identify the system while the airspeed and the baseline collective pitch change. The effort required to stabilize the system is thus of the same order of magnitude of the disturbance that the controller introduces to be able to identify the system.

5 Concluding Remarks

The modeling of hydraulic components, and the capability to model the detailed dynamics of the hydraulic controls of a rotorcraft have been added to a multibody, multidisciplinary code developed at the Department of Aerospace Engineering of the *Politecnico di Milano*. The formulation has been presented with details of the modelling of the pipelines by a finite volume approach. A complete set of hydraulic components has been discussed, and detailed where required, to illustrate the capabilities of the proposed formulation. Significant examples from the literature have been discussed, and some analyses performed on a model of the WRATS tiltrotor test stand have been presented, illustrating how the hydraulic formulation fits in the multibody analysis of complex, multidisciplinary problems involving the control of rotorcrafts in critical conditions. Future developments will involve the use of the proposed modeling to determine the system properties in terms of transfer functions to be used in the preliminary design of the control system, and the introduction of more sophisticated constitutive laws to allow the detailed analysis of transient phenomena, including the deformability of the pipes.

Acknowledgements

The authors wish to acknowledge the significant contribution of Mr. Lamberto Puggelli to the implementation of the hydraulic components.

References

- [1] Massimiliano Lanz, Pierangelo Masarati, and Paolo Mantegazza. Unconditionally stable multi-step integration of ordinary differential equations with controlled algorithmic dissipation for multibody dynamics applications. to be published.
- [2] Gian Luca Ghiringhelli, Pierangelo Masarati, Paolo Mantegazza, and Mark W. Nixon. Multi-body analysis of a tiltrotor configuration. *Nonlinear Dynamics*, 19(4):333–357, August 1999.
- [3] Gian Luca Ghiringhelli, Pierangelo Masarati, and Paolo Mantegazza. A multi-body implementation of finite volume beams. *AIAA Journal*, 38(1):131–138, January 2000.
- [4] Pierangelo Masarati. *Comprehensive Multibody AeroServoElastic Analysis of Integrated Rotorcraft Active Controls*. PhD thesis, Dipartimento di Ingegneria Aerospaziale, Politecnico di Milano, Milano, Italy, 1999.
- [5] Herbert E. Merritt. *Hydraulic Control Systems*. John Wiley & Sons, New York, 1967.
- [6] Robert Piché and Asko Ellman. A fluid transmission line model for use with ode simulators. In *Eight Bath International Fluid Power Workshop*, Bath, UK, September 20–22 1995.
- [7] Jari Mäkinen, Asko Ellman, and Robert Piché. Dynamic simulations of flexible hydraulic-driven multibody systems using finite strain beam theory. In *Fifth Scandinavian International Conference on Fluid Power*, Linköping, 1997.
- [8] Gian Luca Ghiringhelli, Pierangelo Masarati, Paolo Mantegazza, and Mark W. Nixon. Multi-body analysis of an active control for a tiltrotor. In *CEAS Intl. Forum on Aeroelasticity and Structural Dynamics 1999*, pages 149–158, Williamsburg, VA, June 22–25 1999.
- [9] Thomas B. Settle and David L. Kidd. Evolution and test history of the V-22 0.2-scale aeroelastic model. *Journal of the American Helicopter Society*, 37(1):31–45, January 1992.
- [10] K. W. Eure and Jer-nan Juang. Broadband noise control using predictive techniques. TM 110320, NASA, 1997.